Punaglandins, Chlorinated Prostaglandins, Function as Potent Michael Receptors To Inhibit Ubiquitin Isopeptidase Activity

Sheryl M. Verbitski,[†] James E. Mullally,[†,‡] Frank A. Fitzpatrick,[†,‡] and Chris M. Ireland*[,†]

Department of Medicinal Chemistry, University of Utah, 30 South 2000 East, Skaggs Hall, Room 307, Salt Lake City, Utah 84112, and Huntsman Cancer Institute, University of Utah, 2000 Circle of Hope, Salt Lake City, Utah 84112

Received September 9, 2003

Cyclopentenone prostaglandins exhibit unique antineoplastic activity and are potent growth inhibitors in a variety of cultured cells. Recently the dienone prostaglandin, Δ^{12}-PGJ_2, was shown to preferentially inhibit ubiquitin isopeptidase activity of the proteasome pathway. It is theorized that isopeptidase inhibition and general cytotoxicity of prostaglandins depend on olefin−ketone conjugation, electrophilic accessibility, and the nucleophilic reactivity of the endocyclic β-carbon. Δ^{12}-PGJ_2, which contains a cross-conjugated α,β-unsaturated ketone, was a potent inhibitor of isopeptidase activity, whereas PGA_1 and PGA_2 with simple α,β-unsaturated pentenones were significantly less potent and PGB_1 with a sterically hindered α,β-unsaturated ketone was inactive. To further investigate the proposed mechanism, punaglandins, which are highly functional cyclopentadienone and cyclopentenone prostaglandins chlorinated at the endocyclic α-carbon position, were isolated from the soft coral *Telesto riisei*. They were then assayed for inhibition of ubiquitin isopeptidase activity and antineoplastic effects. The punaglandins were shown to inhibit isopeptidase activity and exhibit antiproliferative effects more potently than A and J series prostaglandins. Also, the cross-conjugated dienone punaglandin was more potent than the simple enone punaglandin. The ubiquitin−proteasome pathway is a vital component of cellular metabolism and may be a suitable target for antineoplastic agents. These newly characterized proteasome inhibitors may represent a new chemical class of cancer therapeutics.

The prostaglandins (PGs), a class of intracellular second messengers comprising C_{20}-unsaturated polyoxygenated fatty acids, exhibit distinct biological activity that is determined by structure nuances.[1,2] The cyclopentenone PGs have unique antineoplastic activity and are potent growth inhibitors in a variety of cultured cells. Although most PGs bind specific G-protein-coupled prostanoid receptors that alter adenosine 3′,5′-monophosphate (cAMP) concentrations to produce a biological response, the cyclopentenone PGs exhibit activity by binding other cellular targets without affecting cAMP concentrations.[3−5] Recently Δ^{12}-PGJ_2 (**1**) (Figure 1), an electrophilically active PG containing an accessible cross-conjugated α,β-unsaturated ketone, was shown to preferentially inhibit ubiquitin−isopeptidase activity of the 26S proteasome pathway.[6]

The proteasome system is a key component of the intracellular-protein degradation system, degrading most proteins in the cytosol and nucleus.[7] Protein degradation through a selective and programmed system is an essential component of cell-cycle progression. Specific proteins are targeted for degradation by the 26S proteasome through polyubiquitin−protein ligation.[8] This ligation requires an initial supply of monomeric ubiquitin (Ub), which is regulated by a large family of cysteine proteases, the ubiquitin isopeptidases (ubiquitin-specific proteases). After proteasome proteolysis, ubiquitin isopeptidases disassemble polyubiquitin and ubiquitin-protein remnants into reusable monomers by

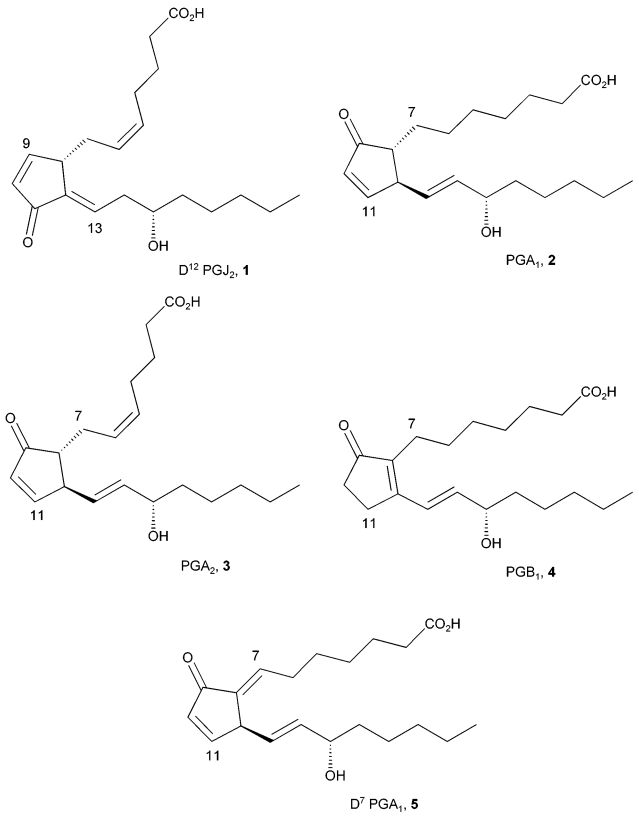

Figure 1. Chemical structures of prostaglandins.

* To whom correspondence should be addressed. Phone: 801-581-8305. Fax: 801-585-6208. E-mail: cireland@pharm.utah.edu.
[†] Department of Medicinal Chemistry.
[‡] Huntsman Cancer Institute.

10.1021/jm030448l CCC: $27.50
Published on Web 03/11/2004

cleaving the isopeptide bonds between the C-terminal carboxyl of ubiquitin and the ϵ-amino group of a lysine residue of another ubiquitin or of the protein remnant.[8−10] This ubiquitin disassembly replenishes the intracellular ubiquitin supply for repeated conjugation to new substrates.[9,10] Although little is known about these enzymes, their importance is undisputed. Their ability to degrade polyubiquitin and replenish the free Ub pool is essential for the function of the proteasome and the viability of the cell.

The mechanism proposed for Δ^{12}-PGJ$_2$ (**1**) mediated inhibition of isopeptidase activity is nucleophilic addition, perhaps by a thiol to the PG's endocyclic β-carbon. It is also theorized that propensity toward this addition reaction is related to the PG's olefin−ketone conjugation and electrophilic accessibility.[6]

Evidence of olefin−ketone conjugation and electrophilic accessibility influencing biological activity can be observed with isopeptidase inhibition activity. Interestingly, only the dienone Δ^{12}-PGJ$_2$ (**1**) with two sterically accessible β-carbons was a potent inhibitor of isopeptidase activity, whereas the simple enones PGA$_1$ (**2**) and PGA$_2$ (**3**) (Figure 1) with only one reactive β-carbon were significantly less potent.[6] The enone PGB$_1$ (**4**) (Figure 1) containing a sterically hindered Michael receptor did not inhibit isopeptidase activity.[6] Additionally, other cross-conjugated α,β-unsaturated carbonyl compounds containing two accessible β-carbons that are chemically unrelated to PGs have been shown to inhibit isopeptidase activity.[11]

This olefin−ketone conjugation effect has also been correlated to antiproliferative activity. It has previously been demonstrated that a cross-conjugated cyclopentadienone system is essential for potent antitumor activity in the PGs. PGs containing a simple enone have been shown to be significantly less effective in this regard.[3,12,13] For example, murine leukemia cells (L1210) are 5-fold more sensitive toward Δ^{12}-PGJ$_2$ (**1**) than PGA$_2$ (**3**).[14] Interestingly, the synthetic PGA series analogue, Δ^{7}-PGA$_1$ (**5**) (Figure 1), which contains a dienone constituent, has 5-fold greater antitumor activity than Δ^{12}-PGJ$_2$ (**1**).[15] Since it is postulated that the electrophilic β-carbon of α,β-unsaturated PGs dictates PG's biological effects via nucleophilic substitution, it is reasonable to hypothesize that chemically altering the reactivity of this carbon toward nucleophiles would have a profound effect on activity. It has been demonstrated that electron-withdrawing substituents such as halogen substitution at the α-carbon of α,β-unsaturated carbonyl compounds enhance Michael addition reactions with nucleophiles.[16,17] One would predict that PGs with an electron-withdrawing group at the endocyclic α-carbon would be more susceptible to nucleophilic attack and would therefore exhibit increased inhibition of ubiquitin−isopeptidase activity and enhanced antiproliferative effects.

In 1985, the punaglandins (PNG) chlorinated at C-10, the endocyclic α-carbon, were first isolated from an octocoral *Telesto riisei* (family Telestidae) collected in Hawaii.[18,19] The punaglandins have been shown to exhibit antiinflammatory and antitumor activity.[19,20] Interestingly, punaglandins possessing a cross-conjugated enone displayed 1 order of magnitude increased potency over the clavulones, also a cross-conjugated

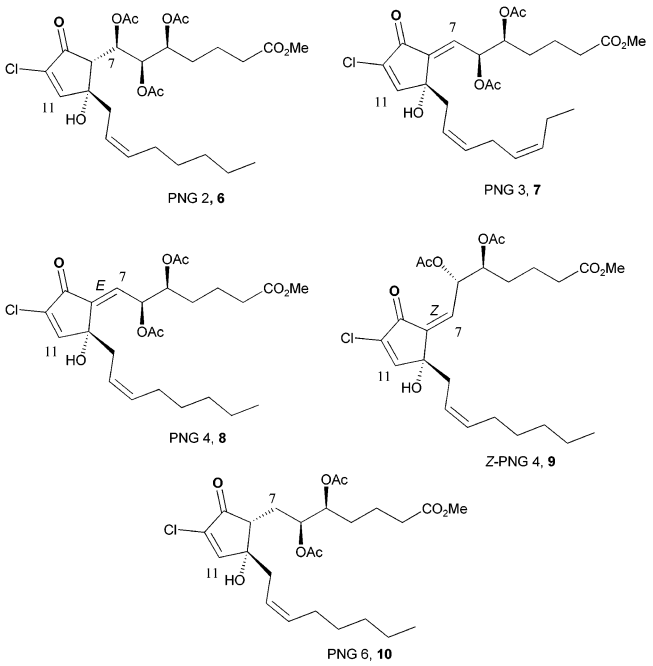

Figure 2. Chemical structures of punaglandins.

cyclopentadienone but devoid of Cl, in mouse leukemia cells with IC$_{50}$ values of 0.03 versus 0.6 μM, respectively.[20,21] On the basis of the assumption that the C-10, Cl substituent may lead to increased antimitotic activity, Dominguez et al. synthesized halogenated prostaglandin derivatives devoid of a 7,8-olefin and tested them for inhibitory effects on leukemia cell proliferation.[22] The nonhalogenated starting material produced no significant inhibitory activity. In contrast, the halogenated (Cl, Br, and I) derivatives displayed potent inhibitory effects in the μg/mL range.[22] To test our hypothesis, various punaglandins (Figure 2) were isolated and examined for enhanced ubiquitin−isopeptidase inhibition and antiproliferative effects when compared to J and A series PGs.

Chemistry

Isolation of Punaglandins. The octocoral, *Telesto riisei* was collected in Hawaii, August 2001. The freeze-dried organism was macerated and subjected to a hexane−Soxhlet extraction.[19] The hexane-soluble material was partitioned against 70% CH_3OH/30% H_2O, resulting in hexane and aqueous CH_3OH fractions. The ^{1}H NMR spectrum confirmed the presence of punaglandins in the aqueous fraction. The aqueous-soluble material was subjected to silica gel flash chromatography, yielding three fractions containing mixtures of punaglandins as determined by ^{1}H NMR. Each fraction was further purified by reversed-phase C-18 HPLC leading to the following punaglandins: PNG 2 (**6**), PNG 3 (**7**), PNG 4 (**8**), *Z*-PNG 4 (**9**), and PNG 6 (**10**) (Figure 2).

Structure Determination of Punaglandins. The structures of the punaglandins were confirmed by ^{1}H and ^{13}C NMR and EIMS. Additionally, HMQC, HMBC, and DEPT data were collected for PNG 2 (**6**), *Z*-PNG 4 (**9**), and PNG 6 (**10**). All data were consistent with literature values.[19] ^{1}H and ^{13}C NMR and EIMS data are provided in the Experimental Section.

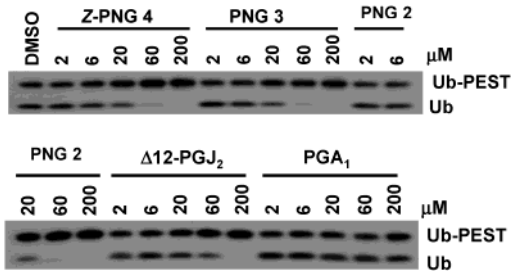

Figure 3. Western blot showing in vitro isopeptidase inhibition of PNG 2 (**6**), PNG 3 (**7**), *Z*-PNG 4 (**9**), Δ^{12}-PGJ_2 (**1**), and PGA_1 (**2**). Isopeptidase inhibition was measured as an increase in the amount of isopeptidase substrate Ub−PEST and a decrease in the amount of cleaved Ub monomer.

Biological Results

Isopeptidase Assay. We hypothesized that the punaglandins would inhibit ubiquitin−isopeptidase activity of the proteasome pathway as does the prostaglandin Δ^{12}-PGJ_2 (**1**) but with greater potency because of chlorination at C-10. To validate this theory, cellular isopeptidase enzymatic activity was measured in vitro after treatment with individual punaglandins, PNG 2 (**6**), PNG 3 (**7**), and *Z*-PNG 4 (**9**) and in vivo after individual treatment with PNG 4 (**8**) and PNG 6 (**10**). This activity was determined utilizing the simple isopeptidase substrate, ubiquitin−PEST (Ub−PEST), a full-length ubiquitin molecule fused with an 18-amino acid C-terminal peptide extension that most isopeptidases use as a substrate.[23,24] The polypeptide extension contains regions rich in Pro (P), Glu (E), Ser (S), and Thr (T) residues called PEST motifs that are responsible for rapid degradation of these and other unstable proteins.[23] Ub isopeptidases specifically cleave this peptide extension, yielding free, full-length Ub. Both the fused Ub−PEST (10.5 kDa) and the cleaved, free Ub (8.5 kDa) can be observed via immunochemical detection.

In Vitro Isopeptidase Activity. PNG 2 (**6**), PNG 3 (**7**), and *Z*-PNG 4 (**9**) were initially analyzed for isopeptidase activity in vitro in HCT 116 lysates. Cells were lysed with isopeptidase activity buffer, and the protein concentration was adjusted to 0.3 mg/mL per sample. Each sample was subsequently incubated with 2, 6, 20, 60, or 200 μM of PNG 2 (**6**), PNG 3 (**7**), *Z*-PNG 4 (**9**), Δ^{12}-PGJ_2 (**1**), or PGA_1 (**2**) in addition to 50 μg/mL of Ub−PEST. Negative control cells were treated with vehicle (0.5% DMSO) and equivalent Ub−PEST. The reaction was terminated after 45 min, a time point that was previously determined to demonstrate Ub−PEST degradation (data not shown). The amount of fused Ub−PEST and free Ub product was determined by SDS−PAGE fractionation (Figure 3).

The results were as anticipated. The vehicle control cells revealed a 1:1 ratio of fused Ub−PEST (10.5 kDa) to free Ub (8.5 kDa) as predicted to occur at a 45 min time interval. The simple dienone PGA_1 (**2**) showed no detectable inhibition of Ub−PEST degradation and was comparable to vehicle-treated lysates. Δ^{12}-PGJ_2 (**1**) inhibited Ub−PEST degradation initially at 60 μM with apparent total inhibition at 200 μM. These results are in agreement with previously reported data for **1**.[6] The punaglandins also inhibited Ub−PEST degradation. Inhibition was initially observed at 20 μM with complete inhibition occurring at 60 μM, indicating that PNG 2 (**6**), PNG 3 (**7**), and *Z*-PNG 4 (**9**) are more potent inhibitors of isopeptidase activity in vitro than Δ^{12}-PGJ_2 (**1**).

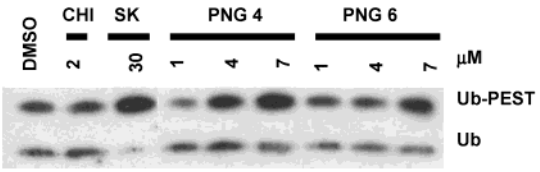

Figure 4. Western blot showing in vivo isopeptidase inhibition by PNG 4 (**8**) and PNG 6 (**10**). Isopeptidase inhibition was determined from an increase of isopeptidase substrate Ub−PEST and a decrease in cleaved Ub monomer.

In Vivo Isopeptidase Activity. To investigate whether punaglandins can inhibit isopeptidase activity in vivo, isopeptidase activity was analyzed after punaglandin treatment of RKO cells. PNG 4 (**8**) and PNG 6 (**10**) were selected for in vivo investigation because they differ only in enone functionality, where **8** is a dienone and **10** is an enone. RKO cells were incubated with 1, 4, or 7 μM of PNG 4 (**8**) or PNG 6 (**10**). As a negative control, cells were incubated with vehicle (0.5% DMSO) or the protein synthesis inhibitor cycloheximide (CHI), which does not inhibit isopeptidase activity. As a positive control, cells were treated with a known isopeptidase inhibitor, shikoccin (SK). After 6 h of drug treatment, cells were lysed and protein concentration was adjusted to 0.3 mg/mL per sample. Each sample was subsequently incubated with 50 μg/mL of Ub−PEST. The reaction was terminated after 20 min, and the respective amounts of Ub−PEST (10 kDa) and free Ub product (8.5 kDa) were determined by SDS−PAGE fractionation (Figure 4).

The in vivo data confirmed isopeptidase inhibition by PNG 4 (**8**) and PNG 6 (**10**). Control cells treated with vehicle or cycloheximide produced an approximately 2:1 ratio of Ub−PEST to free Ub similar to no treatment (data not shown). The positive control, shikoccin, showed expected inhibition of Ub−PEST degradation as did **8** and **10** with noticeable inhibition occurring at 7 μM. Previous in vivo studies of Δ^{12}-PGJ_2 (**1**) in cells treated for 12 h showed inhibition of Ub−PEST degradation at 60 μM.[25] This in vivo data correspond well with the in vitro data, suggesting that PNG 4 (**8**) and PNG 6 (**10**) inhibit isopeptidase activity in vivo more potently than Δ^{12}-PGJ_2 (**1**). Densitometry measurements verified that Ub−PEST degradation at 7 mM for **8** is 67% of the control compared to 75% for **10**.

p53 Independence. Proteasome inhibitors cause rapid accumulation of substrates normally degraded by the ubiquitin−proteasome pathway.[26] For instance, p53 and p53-inducible gene products such as p21 are regulated by this pathway. The ubiquitin proteasome−pathway post-transcriptionally regulates the cellular amount of p53 via murine double minute-2 (MDM2) that directly interacts with p53 promoting its ubiquitination and proteasomal degradation.[27,28] p53 is typically latent until activated by cellular stress or DNA damage, which causes disruption of the p53−MDM2 complex. Once dissociated, p53 accumulates and binds DNA, initiating transcription of genes that trigger growth arrest, DNA repair, and apoptosis.

Characteristic of proteasome pathway inhibitors, treatment of cells with Δ^{12}-PGJ_2 (**1**) inhibits degradation

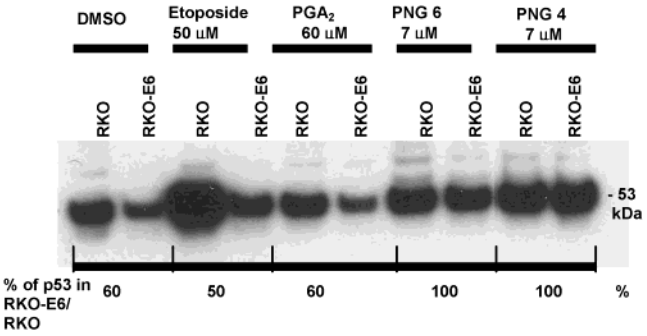

Figure 5. Western blot showing p53 accumulation in RKO and RKO-E6 cells treated with PNG 6 (**10**) and PNG 4 (**8**). Percent of p53 in RKO-E6 cells compared to RKO cells was determined by densitometry.

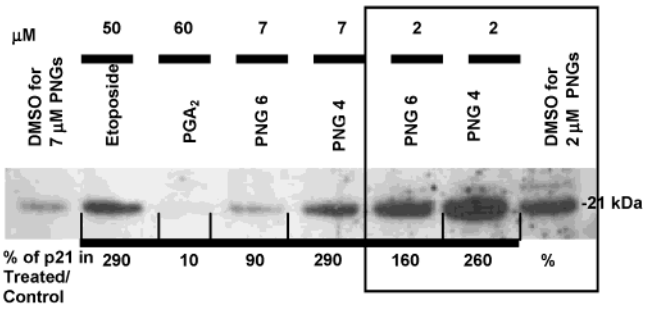

Figure 6. Western blot showing p21 accumulation in RKO cells treated with PNG 6 (**10**) and PNG 4 (**8**). Blocked area shows 2 mM PNG samples and corresponding DMSO control, and unblocked area is 7 mM PNG samples and corresponding controls. Percent of p21 in treated cells compared to control cells was determined by densitometry.

of the tumor-suppressor protein p53, causing it to accumulate in cells.[6] Since punaglandins also inhibit ubiquitin isopeptidase activity, we hypothesized that PNG 4 (**8**) and PNG 6 (**10**) also inhibit p53 degradation by inhibiting its proteasomal degradation. To determine if our hypothesis was correct, both PNGs were assayed in isogenic colon cancer cell lines RKO and RKO-E6. RKO-E6 cells are isogenic variants of RKO cells stably transfected with the HPV-E6 (human papilloma virus derived E6) oncoprotein. The E6 viral oncoprotein recruits and binds a cellular ubiquitin-protein ligase E6-AP (E6-associated protein).[29] This E6-AP complex specifically interacts with p53, targeting it for ubiquitin−proteasome-mediated degradation, thus increasing degradation of p53.[30,31] Generally, p53 levels are significantly lower in RKO-E6 cells compared to RKO cells because of increased degradation of p53. When these cells are treated with ubiquitin−proteasome pathway inhibitors, p53 accumulates in RKO and RKO-E6 cells to a similar extent.

To determine if punaglandins inhibit p53 degradation by disrupting the proteasome pathway, the accumulation ratio of p53 was determined in RKO and RKO-E6 cells treated with selected punaglandins, PNG 4 (**8**) and PNG 6 (**10**). Equally seeded RKO and RKO-E6 cells were treated with vehicle (0.5% DMSO), 50 μM etoposide, 60 μM PGA_2 (**3**), 7 μM PNG 6 (**10**), or 7 μM PNG 4 (**8**). After 6 h of incubation with vehicle or drug, cells were lysed and harvested. An amount of 15 μg/mL of protein from each lysate was fractionated by SDS−PAGE and probed for p53 protein (Figure 5). The p53 band intensities were then analyzed and quantitated using densitometry. The ratio of p53 in RKO-E6 to RKO cells was calculated by dividing the amount of p53 in RKO-E6 cells by the amount in RKO cells and multiplying by 100 to give the percentage (Figure 5).

Control RKO-E6 cells (vehicle-treated) show less accumulated p53 protein than the control RKO (60%) as expected because of RKO-E6's specifically enhanced p53 degradation (Figure 5). Also, etoposide, a topoisomerase II inhibitor that induces p53 activation but does not inhibit the proteasome pathway, was examined in the RKO and RKO-E6 cell lines. Because of increased p53 degradation by E6, less p53 accumulated in RKO-E6 cells compared to RKO cells (50%). PGA_2 (**3**), an enone PG that negligibly inhibits isopeptidase activity, shows results comparable to the control treatment with regard to p53 accumulation in RKO-E6 cells at 60% of RKO cells. As hypothesized, PNG 6 (**10**) and PNG 4 (**8**) assayed at a lower concentration of 7 μM versus Δ^{12}-PGJ_2 (**1**), assayed at 60 μM (data not shown),[6] showed enhanced accumulation of p53 in the RKO and RKO-E6 cells. This enhanced accumulation of the proteasomal regulated p53 protein in both cell lines is consistent with activity expected of ubiquitin-isopeptidase inhibitors. It is interesting to note that although the enone PNG 6 (**10**) induces significant p53 accumulation in both cell lines, there appears to be slightly less accumulation in the RKO-E6 cell line.

p21 Accumulation. The dienone prostaglandin, Δ^{12}-PGJ_2 (**1**), and the enone PGs, PGA_1 (**2**) and PGA_2 (**3**), have been shown to electrophilically alter wild-type p53 conformation, causing accumulation of transcriptionally silent p53 in the cytosol.[6,32] This inactivation of p53 eliminates p53-dependent transactivation of $p21^{Waf/Cip-1}$ (p21).[32] RKO and HCT 116 cells treated with PGA_1 (**2**) and PGA_2 (**3**) show an increase in mutant p53 protein levels and a decrease in p21 mRNA transcription and p21 protein induction.[6,32] Unlike the enones **2** and **3**, the dienone Δ^{12}-PGJ_2 (**1**) causes a decline in p21 mRNA but an increase in accumulated p21 protein.[6] This differential activity is attributed to Δ^{12}-PGJ_2's ability to preferentially inhibit ubiquitin-isopeptidase activity via its cross-conjugated α,β-unsaturated ketone, thus decreasing transcription and degradation of p21.[32]

It was therefore hypothesized that the isopeptidase inhibitors PNG 4 (**8**) and PNG 6 (**10**) would cause a similar accumulation of p21 protein. RKO cells were treated with 2 and 7 μM of **8** and **10**, 50 μM etoposide, 60 μM PGA_2 (**3**), or 0.5% DMSO for 6 h before harvesting. Protein was then quantitated, fractionated by SDS−PAGE, and probed for p21 protein (Figure 6). The p21 band intensities were then analyzed and quantitated using densitometry. The ratio of p21 in treated cells to control cells was calculated by dividing the amount of p21 in treated cells by the amount in control cells and multiplied by 100 to give percent (Figure 6).

DMSO-treated controls exhibit negligible accumulation of p21 protein, and etoposide shows significant induction of p21, 290% over control. Also, treatment with the enone PGA_2 (**3**) almost completely abrogates p21, to 10% of the control. The punaglandins show p21 accumulation, 90−290% of control. Notably, the enone punaglandin PNG 6 (**10**) shows significantly less p21 accumulation than the dienone PNG 4 (**8**).

Caspase Assay. Another characteristic function of isopeptidase inhibitors is their ability to cause apoptosis

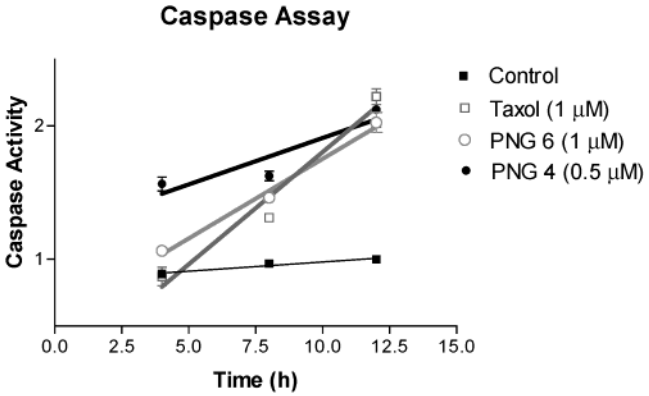

Figure 7. Graph of caspase-3 activity versus time used to determine apoptosis. Caspase-3 activity of PNG 6 (**10**) and PNG 4 (**8**) rose steadily in treated cells, indicating apoptosis.

independently of p53.[6,11] Mammalian cells undergo apoptosis during normal development or in response to a variety of stimuli. The involvement of the ubiquitin−proteasome in apoptosis has been established, yet its precise role remains unresolved. It is most likely linked to its ability to degrade cellular proteins that are intimately involved in apoptosis regulation. In most cell lines, proteasome inhibitors have been shown to trigger apoptosis upstream of the caspase cascade.[33] Although both the dienone Δ^{12}-PGJ_2 (**1**) and enone PGs, PGA_1 (**2**) and PGA_2 (**3**), have been shown to alter p53 protein conformation in RKO and HCT 116 cells, only the isopeptidase-inhibitor prostaglandin Δ^{12}-PGJ_2 (**1**) potently causes apoptosis independently of p53.[6,32]

The J series prostaglandins have been shown to induce apoptosis in a time-dependent manner in RKO cells.[6] To determine if selected punaglandins PNG 4 (**8**) and PNG 6 (**10**) also induce apoptosis in RKO cells in a time-dependent manner, caspase-3 activity was determined. During apoptosis, the caspases, a family of cysteinyl aspartate specific proteases, are activated.[34] These enzymes cleave specific substrates, resulting in biochemical and morphological changes associated with apoptosis. Therefore, detection of activated caspases can be used as a biochemical marker for apoptosis. Caspase-3 has substrate specificity for the amino acid sequence Asp-Glu-Val-Asp (DEVD), cleaving after Asp, and therefore, caspase-3 activity can be measured by monitoring cleavage of the substrate DEVD-AMC (Asp-Glu-Val-Asp-7-amino-4-aminomethylcoumarin).

RKO cells were treated for 4, 8, and 12 h with PNG 4 (**8**) at 0.5 μM and PNG 6 (**10**) at 1 μM. Taxol, a known apoptotic inducer at 1 μM, was used as a positive control, and negative control cells were treated with vehicle (0.5% DMSO). Caspase-3 activity rose steadily as expected from 4 to 12 h in cells treated with PNG 4 (**8**), PNG 6 (**10**), and Taxol but remained constant in the untreated control cells (Figure 7). These results confirm that both the dienone PNG 4 (**8**) and the enone PNG 6 (**10**) cause apoptosis in RKO cells.

Cytotoxicity in Human Colon Tumor (HCT) Cell Lines. To determine if punaglandins elicit cytotoxicity independently of the tumor-suppressor p53, as do other dienone prostaglandins, several cytotoxicity assays were employed. First, cell death effects of all punaglandins were investigated in pairs of isogenic colon cancer cell lines, the HCT $116^{+/+}$ competent cell line, and HCT $116^{-/-}$ null cell lines. HCT $116^{+/+}$ cells are homozygous for $p53^{+/+}$ and $p21^{+/+}$, whereas HCT $116^{-/-}$ cells lack both alleles for p53 ($p53^{-/-}$) or p21 ($p21^{-/-}$).

Table 1. Cytotoxicity of Punaglandins in HCT 116 (p53 wt, $p53^{-/-}$, p21 wt, and $p21^{-/-}$) Cell Lines

	EC_{50}, μM			
compd	HCT 116 (p53wt), μM	HCT 116 ($p53^{-/-}$)	HCT 116 (p21wt)	HCT 116 ($p21^{-/-}$)
6	0.040	0.040	0.047	0.040
7	0.32	0.37	0.29	0.30
8	0.33	0.35	0.34	0.28
9	0.032	0.027	0.030	0.032
10	0.34	0.36	0.33	0.32

Table 2. Cytotoxicity of PNG 4 (**8**) and PNG 6 (**10**) in RKO and RKO-E6 Cell Lines

	EC_{50}, μM	
compd	RKO	RKO-E6
8	0.31	0.37
10	0.44	0.47

Each cell line was seeded simultaneously in 96-well plates and incubated for 24 h before treatment with individual punaglandins at various concentrations for an additional 48 h. Cytotoxicity was determined using MTS, and absorbances were recorded at 490 nm. The log EC_{50} and EC_{50} values were calculated from a concentration−response curve generated using GraphPad Prism (Table 1).

Each punaglandin caused cell death with equal potency and efficacy in HCT 116 $p53^{+/+}$ and $p21^{+/+}$ compared to the corresponding HCT 116 $p53^{-/-}$ and $p21^{-/-}$ null cell lines, respectively (Table 1). These results are indicative of a p53-independent mechanism. Punaglandins are also more potent than PGA_1 (**2**) and Δ^{12}-PGJ_2 (**1**) in competent HCT 116 cells, which display EC_{50} values of 11.6 and 3.6 μM, respectively.[25] Interestingly, PNG 2 (**6**) and *Z*-PNG 4 (**9**) have increased cytotoxicity (EC_{50} = 0.04 and 0.03 μM, respectively) compared to PNG 3 (**7**), PNG 4 (**8**), and PNG 6 (**10**) (average $EC_{50} \approx 0.35$ μM). This result may be due to different spatial orientations of PNG 2 (**6**) and *Z*-PNG 4 (**9**) that exhibit less steric hindrance toward nucleophilic addition. Suzuki et al. suggested that a 1,3-interaction between the C(8) and C(11) substituents on PGA_1 (**2**) may control stereoselectivity of thiol addition at C(11).[13] Perhaps a similar steric interaction exists in **7**, **8**, and **10**, thus slightly decreasing cytotoxicity.

Cytotoxicity in Human Colon Tumor (RKO) Cell Lines. Punaglandins **8** and **10** were also assayed for p53-independent cytotoxicity in RKO and RKO-E6 cells. Each cell line was seeded simultaneously in 96-well plates and incubated for 24 h before treatment with PNG 4 (**8**) and PNG 6 (**10**) at various concentrations for 48 h (Table 2).

The punaglandins caused cell death with equal potency and efficacy in RKO cells (competent p53) and RKO-E6 (disrupted p53) cell lines. These data further substantiate that the cytotoxicity mechanism of the punaglandins is p53-independent. Additionally, PNG 4 (**8**) and PNG 6 (**10**) are more potent in RKO cell lines than PGA_1 (**2**) and Δ^{12}-PGJ_2 (**1**), generating EC_{50} values of 33.6 and 9.0 μM, respectively,[6] versus 0.31 μM for **8** and 0.44 μM for **10**.

Table 3. Actual and Predicted Endocyclic β-^{13}C NMR Shifts Determined by NMR and Molecular Modeling Studies

	endocyclic β-^{13}C NMR shifts, ppm		
compd	actual	predicted	Cl or H substitution
1	162.0	162.2	154.4, Cl substitute
2	165.0	167.5	159.4, Cl substitute
8	155.8	155.5	163.0, H substitute
10	157.5	156.2	166.2, H substitute

Conclusion and Discussion

Accessible electrophilic β-carbons of α,β-unsaturated carbonyls readily react with nucleophiles to form Michael adducts. It has been postulated that this reaction occurs with cyclopentenone PGs selectively at their endocyclic β-position dictating biological effects.[12,13] This reactivity may also be governed by PG olefin−ketone conjugation. It was postulated that electronegative substituents at the α-position of α,β-unsaturated carbonyls in both dienone and enone PGs would increase reactivity toward nucleophilic addition and therefore biological activity. To evaluate this theory, punaglandins, prostaglandins chlorinated at the endocyclic α-carbon, were assayed for inhibition of ubiquitin-isopeptidase activity and antiproliferative effects.

As discussed previously, the dienone PG, Δ^{12}-PGJ$_2$, shows potent isopeptidase inhibition and apoptosis, but the simple enone, PGA$_1$, shows no detectable isopeptidase inhibition or apoptosis. As hypothesized, dienone and enone punaglandins inhibit isopeptidase activity in vitro and in vivo. Additionally the dienone PNG 4 (**8**) and enone PNG 6 (**10**) induced apoptosis in RKO cells. They also displayed cytotoxicity independently of p53 more potently than the nonhalogenated prostaglandin Δ^{12}-PGJ$_2$. Interestingly, the dienone PNG 4 (**8**) is a more potent isopeptidase inhibitor than the enone PNG 6 (**10**). This increased potency was observed in the direct in vivo isopeptidase assay as well the indirect assays detecting p53 and p21 accumulation. These data suggest that PG biological activity is related to its olefin−ketone conjugation as well as reactivity of the endocyclic β-carbon.

It was predicted that the electron-withdrawing Cl substituent of the PNGs reorganizes charge distribution of the α,β-carbonyl system and this reorganization increases reactivity and activity. To deduce the chemical environment about the endocyclic β-carbon, ^{13}C NMR and molecular modeling studies were employed. The chemical shift obtained from NMR experiments is a precise measure of the chemical environment around a nucleus. This nuclear environment or electron density around the nucleus is affected by nearby substituent electronics that can shield or deshield a nucleus from an applied field. In general, the more electropositive the nucleus, the larger its chemical shift.

Although the endocyclic β-^{13}C NMR shifts determined were not dramatically different among compounds **1**, **2**, **8**, and **10**, the results are interesting and may provide valuable insight (Table 3). The enone PGA$_1$ (**2**), which does not possess appreciable isopeptidase-inhibitory activity, has the most downfield shift compared to PNG 4 (**8**), which is the most potent isopeptidase inhibitor in this study.

To make a more direct comparison, molecular modeling studies of Δ^{12}-PGJ$_2$ (**1**), PGA$_1$ (**2**), PNG 4 (**8**), and PNG 6 (**10**) were evaluated along with their theoretical halogenated or nonhalogenated analogues. These studies provided carbon chemical shifts consistent with NMR studies (Table 3). Predicted ^{13}C chemical shifts on the endocyclic α-position shifted an average of 12.5 ppm downfield when substituted with a Cl or 12.5 ppm upfield when substituted with H. Additionally, carbon shifts adjacent to the substitution position, the carbonyl, and the endocyclic β-carbon shifted upfield. Given these studies, it appears that the electron population is altered by the Cl substituent yielding a more net positive charge on the α-position and a more net negative charge on the β-position.

Counterintuitive to NMR studies, previous research shows that addition of thiols such as glutathione to dienone PGs occurs more rapidly and forms more labile thiol conjugates compared to enone PGs.[13] Therefore, dienone reactivity is considered to be under kinetic control and the enone is under thermodynamic control.[12,13] Cross-conjugated dienone PGs readily, yet reversibly, undergo Michael addition reactions with glutathione, generating an equilibrium mixture shifted to the free PG over the conjugated PG.[12,13] The free PG can then directly interact with nuclear or cytosol proteins to produce a biological response. Enone PGs also bind glutathione but in an irreversible manner so the equilibrium favors thiol conjugate formation.[1,13] Glutathione, the most abundant nonprotein source of cellular thiol, reacts with a variety of electrophiles to form glutathione conjugates. Once formed, these glutathione conjugates are eliminated from the cell via the GS-X pump, thus decreasing the cellular accumulation of enone PGs.[13] These PG−glutathione adducts not only are eliminated from the cell but do not exhibit antiproliferative activity.[13] This difference in chemical reactivity toward thiol addition might account for the higher activity of dienone PGs compared to enone PGs and for the PNGs versus the PGs.

From these studies of the chlorinated prostaglandins, the punaglandins have been shown to increase isopeptidase inhibition and antiproliferative activity compared to the nonhalogenated PGs. These newly characterized proteasome inhibitors may represent a new class of potent cancer therapeutics.

Experimental Section

General Chemistry. NMR spectra were recorded on a Varian Mercury 400 MHz spectrometer (^{1}H, 399.880 MHz, ^{13}C, 100.559 MHz) at 25 °C. The ^{1}H and ^{13}C chemical shifts are reported in parts per million (ppm) relative to the reference solvent peaks at δ 7.26 and 77.00 ppm for $CDCl_3$. Mass spectral measurements (EI) were performed on a Finnegan MAT 95 high-resolution spectrometer.

Cell Culture. Human colon tumor cells (HCT 116), wild-type for p53 and p21 expression and isogenic lines in which the p53 or p21 gene was disrupted through homologous recombination (gift from Dr. Bert Vogelsein, Johns Hopkins University, Baltimore, MD), were maintained in McCoy's 5A medium supplemented with 2 mM L-glutamine, 1 mM MEM-sodium pyruvate, 50 units/mL penicillin and streptomycin, and 10% (v/v) fetal bovine serum (FBS). Human colon tumor cells, RKO and RKO-E6 cells (gift from Dr. Mark Meuth, Institute, University of Sheffield, Sheffied, U.K.), were maintained in Dulbecco's modified Eagle medium supplemented with 2 mM L-glutamine, 1 mM MEM-sodium pyruvate, 50 units/mL penicillin and streptomycin, and 10% (v/v) FBS. All cell lines were maintained in a humidified incubator at 37 °C and 5% CO_2/air atmosphere.

Collection, Extraction, and Isolation. The soft coral *Telesto riisei* (586 g) was collected and freeze-dried in Hawaii (gift from Dr. Bill Baker, Florida Tech, FL) in August of 2001. The organism was macerated and subjected to Soxhlet extraction with hexane,[19] yielding 4.54 g of extracted material. The hexane-soluble material was partitioned with 70% CH_3OH/30% H_2O, resulting in a hexane (3.61 g) fraction and an aqueous CH_3OH (733 mg) fraction. ^1H NMR data confirmed punaglandins to be in the aqueous fraction. The aqueous CH_3OH (733 mg) soluble material was subjected to silica gel flash chromatography (30 mm × 17 cm) using an isocratic solvent system of 70% hexane/30% EtOAc. Fractions 5−7 contained mixtures of various punaglandins determined by ^1H NMR analysis. Each fraction was purified by reversed-phase C-18 HPLC (DYNAMAX-60 Å, 8 μm, 10 mm i.d. × 250 mm long; 4.0 mL/min) with a stepwise gradient at 5 min from 70% CH_3OH/30% H_2O to 100% CH_3OH over 15 min, yielding punaglandin 2 (**6**, 29.2 mg), punaglandin 3 (**7**, 29.0 mg), punaglandin 4 (**8**, 10.6 mg), *Z*-punaglandin 4 (**9**, 19.9 mg), and punaglandin 6 (**10**, 4.0 mg). HPLC was used to confirm the purity of each compound.

Punaglandin 2 (6): yellow oil; ^1H NMR (400 MHz, $CDCl_3$) δ 0.88 (3H, t, H20), 1.25 (2 H, m, H18,) 1.28 (2H, m, H19), 1.34 (2H, m, C17), 1.60 (2H, m, H4), 1.67 (2 H, m, H3), 2.00 (2H, m, H16), 2.09 (3H, s, H_3−OAc), 2.12 (3H, s, H_3−OAc), 2.32 (2H, m, H2), 2.47 (2H, m, H13), 2.76 (1H, d, H8), 3.67 (3H, s, H_3−OMe), 5.20 (1H, ddd, H5), 5.28 (1H, ddd, H14), 5.65 (1H, dt, H15), 7.29 (1H, s, H11); ^{13}C NMR (400 MHz, $CDCl_3$) δ 14.0 (C20), 20.0 (C3), 20.7 (CH_3), 20.8 (CH_3), 20.9 (CH_3), 22.5 (C19), 27.4 (C16), 29.0 (C17), 29.9 (C4), 31.5 (C18), 33.3 (C2), 39.9 (C13), 51.7 (CH_3O), 53.3 (C8), 69.9 (C7), 71.4 (C5), 72.7 (C6), 76.5 (C12), 120.8 (C14), 135.9 (C10), 136.7 (C15), 158.1 (C11), 170.2 (CH_3CO), 170.4 (CH_3CO), 173.6 (C1), 195.8 (C9); EIMS (70 eV) *m*/*z* 387 (12), 327 (8), 285 (5), 43 (100); (+)-HRESIMS *m*/*z* 581.2139 ($C_{27}H_{39}O_{10}ClNa$ $[M + Na]^+$ requires 581.2129). The material was purified to a single peak by HPLC, and all collected data were consistent with reported literature values.[19]

Punaglandin 3 (7): yellow oil; ^1H NMR (400 MHz, $CDCl_3$) δ 0.95 (3H, t, H20), 1.64 (4H, m, H3, H4), 2.04 (2H, m, H19), 2.05 (3H, s, H_3−OAc), 2.10 (3H, s, H_3−OAc), 2.32 (2H, m, H2), 2.47 (2H, m, H13), 2.70 (1H, dd, H13b), 2.75, (2H, dd, H16), 3.02 (1H, dd, H13a), 3.65 (3H, s, H_3−OMe), 5.23 (1H, m, H5), 5.26 (1H, m, H5, H14), 5.39 (1H, m, H18), 5.53 (1H, m, H15), 6.04 (1H, dd, H6), 6.37 (1H, d, H7), 7.28 (1H, s, H11); EIMS (70 eV) *m*/*z* 387 (25), 376 (5), 358 (11), 327 (100), 267 (25), 258 (42), 235 (26) 43 (44); (+)-HRESIMS *m*/*z* 519.1758 ($C_{25}H_{33}O_8ClNa$ $[M + Na]^+$ requires 519.1762). The material was purified to a single peak by HPLC, and all collected data were consistent with reported literature values.[19]

Punaglandin 4 (8): yellow oil; ^1H NMR (400 MHz, $CDCl_3$) δ 0.88 (3H, t, J = 7.1, H20), 1.28 (7H, m, H17, H18, H19), 1.64 (4H, m, H3, H4), 2.00 (2H, m, H16), 2.05 (3H, s, H_3−OAc), 2.12 (3H, s, H_3−OAc), 2.32 (2H, m, H2), 2.67 (1H, dd, J = 7.2, 14.5 Hz), 3.00 (1H, dd, J = 8.4, 14.5 Hz, H13b), 3.65 (3H, s, H_3−OMe), 5.28 (2H, m, H5, H14), 5.56 (1H, dt, J = 7.3, 10.8 Hz, H15), 6.04 (1H, dd, J = 4.4, 9.1 Hz, H6), 6.37 (1H, dd, J = 0.9, 9.1 Hz, H7), 7.28 (1H, s, H11); ^{13}C NMR (400 MHz, $CDCl_3$) δ 14.0 (C20), 20.6 (C3), 20.9 (CH_3), 20.9 (CH_3), 22.6 (C19), 27.4 (C16), 29.1 (C17), 29.6 (C4), 31.5 (C18), 33.3 (C2), 35.7 (C13), 51.8 (CH_3O), 69.9 (C5), 73.8 (C6), 77.0 (C12), 121.5 (C14), 130.7 (C7), 135.3 (C15), 137.3 (C10), 140.5 (C8), 155.8 (C11), 169.9 (CH_3CO), 171.2 (CH_3CO), 173.9 (C1), 186.8 (C9); EIMS (70 eV) *m*/*z* 387 (2.0), 347 (3.0), 327 (33.5), 285 (6.7), 267 (6.4), 253 (24.5), 235 (11.5), 207 (13.8), 43 (100); (+)-HRESIMS *m*/*z* 521.1931 ($C_{25}H_{35}O_8ClNa$ $[M + Na]^+$ requires 521.1918). The material was purified to a single peak by HPLC, and all collected data were consistent with reported literature values.[19]

Punaglandin *Z*-4 (9): yellow oil; ^1H NMR (400 MHz, $CDCl_3$) δ 0.88 (3H, t, H20), 1.24 (2H, m, H18,) 1.28 (2H, m, H19), 1.32 (2H, m, C17), 1.60 (2H, m, H4), 1.64 (2H, m, H3), 1.98 (2H, m, H16), 2.04 (3H, s, H_3−OAc), 2.11 (3H, s, H_3−OAc), 2.34 (2H, m, H2), 2.45 (1H, dd, H13b), 2.50 (H, dd, H13a), 3.66 (3H, s, H_3−OMe), 5.21 (1H, m, H5), 5.25 (1H, m, H14), 5.58 (1H, dt, H15), 6.08 (1H, d, H7), 7.20 (1H, s, H11); ^{13}C NMR (400 MHz, $CDCl_3$) δ 14.0 (C20), 20.6 (C3), 20.8 (CH_3), 20.9 (CH_3), 22.5 (C19), 27.4 (C16), 29.0 (C17), 29.8 (C4), 31.5 (C18), 33.5 (C2), 37.3 (C13), 51.6 (CH_3O), 70.5 (C6), 73.9 (C5), 76.5 (C12), 121.6 (C14), 135.2 (C15), 135.5 (C7), 138.5 (C10), 140.4 (C8), 153.6 (C11), 170.1 (CH_3CO), 170.5 (CH_3CO), 173.5 (C1), 186.7 (C9); EIMS (70 eV) *m*/*z* 387 (76), 327 (47), 285 (19), 267 (17), 253 (40), 235 (29), 207 (26), 43 (100); (+)-HRESIMS *m*/*z* 521.1934 ($C_{25}H_{35}O_8ClNa$ $[M + Na]^+$ requires 521.1918). The material was purified to a single peak by HPLC, and all collected data were consistent with reported literature values.[19]

Punaglandin 6 (10): yellow oil; ^1H NMR (400 MHz, $CDCl_3$) δ 0.89 (3H, t, J = 6.2, H20), 1.30 (7H, m, H17, H18, H19), 1.64 (4H, m, H3, H4), 1.74 (1H, ddd, J = 1.4, 8.6, 15.0, H7a), 2.03 (2H, m, H16), 2.10 (3H, s, H_3−OAc), 2.11 (3H, s, H_3−OAc), 2.12 (1H, m, H7b), 2.14 (1H, m, H13a), 2.34 (2H, m, H2), 2.67 (1H, dd, J = 4.7, 8.7, H8), 2.80 (1H, ddd, J = 1.4, 8.2, 13.9, H13a), 3.66 (3H, s, H_3−OMe), 5.13 (1H, br d, J = 3.5 Hz, H5), 5.29 (2H, m, H6, H14), 5.68 (1H, dt, J = 7.4, 11.1 Hz, H15), 7.31 (1H, s, H11); ^{13}C NMR (400 MHz, $CDCl_3$) δ 14.0 (C20), 20.6 (C3), 20.9 (CH_3), 21.1 (CH_3), 22.5 (C19), 25.5 (C7), 27.5 (C16), 29.1 (C17), 30.3 (C4), 31.5 (C18), 33.3 (C2), 35.9 (C13), 51.6 (CH_3O), 55.1 (C8), 72.1 (C5), 72.2 (C6), 78.9 (C12), 121.2 (C14), 134.5 (C10), 136.4 (C15), 157.5 (C11), 170.6 (CH_3CO), 170.7 (CH_3CO), 173.6 (C1), 196.7 (C9). EIMS (70 eV) *m*/*z* 409 (6.0), 329 (100), 269 (33.4), 255 (43.2), 107 (24.2), 43 (73.6); (+)-HRESIMS *m*/*z* 523.2080 ($C_{25}H_{37}O_8ClNa$ $[M + Na]^+$ requires 523.2075). The material was purified to a single peak by HPLC, and all collected data were consistent with reported literature values.[19]

In Vitro Isopeptidase Assay. HCT 116 cells were seeded at 3.0×10^5 cells per well into a six-well plate. After a 24 h incubation period, cells were harvested in caspase buffer (25 mM HEPES, 5 mM EDTA, 0.1 % CHAPS, 5 mM ATP, pH 7.5). RKO cell lysates adjusted to 0.3 mg/mL were subsequently incubated with 2, 6, 20, 60, and 200 μM of PNG 2 (**6**), PNG 3 (**7**), *Z*-PNG 4 (**9**), Δ^{12}-PGJ_2 (**1**), PGA_2 (**2**), and 0.5% DMSO in addition to 50 μg/mL of Ub−PEST substrate. The reaction mixture was incubated at 25 °C for 45 min before being terminated by the addition of 20 μL of 2 × Laemmli buffer. Samples were then boiled for 5 min and electrophoresed on a 10−20% Tricine gel at 125 V for 2 h in Novex Tricine SDS running buffer. Protein was then transferred onto a PVDF membrane at 25 V for 2 h using Novex transfer buffer with 20% CH_3OH. The membrane was incubated with monoclonal mouse IgG_1 and anti-human Ub (clone Ubi-1) primary antibody and then subsequently incubated with mouse HRP conjugated secondary antibody. The Ub antibody recognizes both conjugated and unconjugated Ub.

In Vivo Isopeptidase Assay. The in vivo isopeptidase assay was performed in RKO cells seeded at 3.0×10^5 cells per well into a six-well plate. After a 24 h incubation period, cells were incubated with 1, 4, and 7 μM of PNG 4 (**8**) and PNG 6 (**10**), 2 μM cycloheximide, 30 μM shikoccin, and 0.5% DMSO. Cells were harvested in caspase assay (25 mM HEPES, 5 mM EDTA, 0.1% CHAPS, 5 mM ATP, pH 7.5), and protein was quantitated using the Bradford method. Protein concentration was adjusted to 0.3 mg/mL, and each sample was incubated with 50 μg/mL of Ub−PEST substrate at 25 °C for 20 min before the reaction was terminated with 20 μL of 2 × Laemmli buffer. Samples were then boiled for 5 min and electrophoresed on a 10−20% Tricine gel at 125 V for 2 h using Novex Tricine SDS running buffer. Protein was subsequently transferred onto a PVDF membrane at 25 V for 2 h using Novex Transfer buffer with 20% CH_3OH. The membrane was incubated with monoclonal mouse IgG_1 and anti-human Ub (clone Ubi-1) primary antibody and then subsequently incubated with mouse HRP conjugated secondary antibody.

Growth Inhibition Assay. Cells were plated in 96-well culture plates in 190 μL of appropriate medium in the following cell amounts per well: HCT 116, 3.0×10^3; RKO and RKO-E6, 5.0×10^3. Plates were incubated for 24 h to allow complete cellular adhesion. Drug was added at varying concentrations in 10 μL of appropriate medium and tested in eight replicates.

Control lanes were treated with comparable DMSO amounts, and a standard drug of interest was tested to validate results. After a 48 h incubation of treated cells, medium and drug were aspirated and 120 μL of a solution of 20 μL of MTS and 100 μL of fresh medium was added. Plates were incubated for 2−3 h. Absorbances were recorded at 490 nm. Each drug treatment's effect was calculated as a percentage of the DMSO control cell growth that was grown in the same culture plate. Data were analyzed, and the effective concentration required to produce a response halfway between maximal response and baseline or 50% maximal effect (EC_{50}), log EC_{50}, and standard errors were calculated using GraphPad Prism 3.02. EC_{50} was calculated as the antilog of the log EC_{50}. The standard error is the calculated log EC_{50}'s standard deviation, which is based on the number of data points collected, each point's distance from the curve, and the overall curve shape. Each assay was performed twice to confirm repeatability.

All punaglandins **6**−**10** at various drug concentrations were evaluated in HCT 116 wt, HCT 116 p53 null, and HCT 116 p21 null cell lines at 48 h. Growth inhibition was determined by measuring viable cells' metabolic conversion of MTS. In addition, growth inhibition assays of selected punaglandins, PNG 4 (**8**) and PNG 6 (**10**), at various concentrations were implemented in RKO and RKO-E6 cell lines for 48 h and determined by measuring the metabolic conversion of MTS.

p53 Induction. RKO and RKO-E6 cells were seeded at 3.0×10^5 cells per well in a six-well plate. After a 24 h incubation period, cells were treated with 7 μM PNG 4 (**8**), 7 μM PNG 6 (**10**), 60 μM PGA_2, 50 μM etoposide, and 1% DMSO for 6 h. After drug treatment, the medium was removed and the cells were lysed in 100 μL of cold lysis buffer (0.05 mM Tris, pH 7.4, 150 mM NaCl, 1 mM EDTA, 1% Triton X-100, 1 mM phenylmethylsulfonyl fluoride (PMSF), 0.1% SDS, 10 μg/mL aprotinin, 10 μg/mL leupeptin, 1 M NaF, 100 mM Na_3VO_4). Protein concentration was measured with the DC protein assay (BioRad Laboratories, Hercules, CA). An amount of 15 μg of sample protein was fractionated by SDS−PAGE at 200 V for 35 min. Protein was then transferred to PVDF membrane and blocked with 5% (w/v) nonfat dry milk in 20 mL of PBS/0.1% Tween at 300 mA for 1.25 h. Proteins were measured immunochemically with mouse monoclonal IgG_{2a} and anti-human p53 (DO-1) primary antibody and then subsequently incubated with mouse HRP conjugated secondary antibody. The p53 antibody recognizes wt and mutant human p53 at the amino terminal epitope mapping between amino acid residues 11 and 25.

p21 Induction. RKO cells were seeded at 3.0×10^5 cells per well in a six-well plate. After a 24 h incubation period, cells were treated with 7 μM PNG 4 (**8**), 7 μM PNG 6 (**10**), 60 μM PGA_2 (**3**), 50 μM etoposide, and 1% DMSO for 6 h. Protein was subjected to immunochemistry as described above in the p53 induction section except proteins were measured with goat polyclonal IgG and anti-human p21 primary antibody and then subsequently incubated with goat HRP conjugated secondary antibody. The p21 antibody used is specific for Ser-146 phosphorylated p21.

Caspase Assay. RKO cells were plated in six-well culture plates at 3.0×10^5 cells per well. Cells were allowed to adhere for 24 h before treatment with 0.5 μM PNG 4 (**8**), 1 μM PNG 6 (**10**), and 1 μM Taxol at 4, 8, and 12 h. After drug pretreatment, the media was removed and centrifuged at 1500 rpm for 5 min. The resulting pellet was rinsed with PBS and centrifuged at 1500 rpm for 5 min. The PBS was removed, and the pellet was saved. The cells were rinsed with cold phosphate-buffered saline (PBS) and then lysed with 250 μL of cold caspase buffer (25 mM Hepes, 5 mM EDTA, 0.1% CHAPS, pH 7.5, 2 mM DTT) for 10 min. The cells were scraped, and the crude lysates were added to the pellet obtained from the removed medium. The lysates were briefly sonicated and then clarified by centrifugation at 10000*g* for 10 min at 4 °C. In a flat-bottom 96-well plate, 45 μL of lysate was added to four individual wells, and as a standard, 45 μL of caspase buffer was added to four separate wells. To each lysate and standard well, 5 μL of 500 μM DEVD-AMC (Asp-Glu-Val-Asp-7-amino-4-aminomethylcoumarin) was added, mixed for 1 min, and incubated at 37 °C for 1 h. After incubation, each sample's fluorescence was recorded in a microplate reader using excitation at 360 nm at 37 °C and emission detection at 460 nm. The protein was quantitated using the Bradford Assay described previously. Caspase activity was calculated with the following equation:

$$\text{caspase activity} = \frac{(F_1/F_{\max})(\text{CS})}{(T)(P)}$$

where F_1 is the fluorescence of the sample, $F_{\max}$ is the maximum fluorescence at 50 000 counts, CS is the amount of cleaved substrate (pmol), T is time (min), and P is the amount of protein sample (μg). The obtained caspase activity was normalized to the control by dividing each caspase activity by the control caspase activity. Results were then graphed using GraphPad Prism.

Molecular Modeling. All calculations were done using Gaussian 98, revision A.11.4, on a Linux cluster. Both geometry optimizations and NMR calculations were DFT using the hybrid B3LYP functional and D95** basis sets on all atoms. The NMR calculations were done using the GIAO method. The resulting chemical shieldings were converted to chemical shifts using the slope and intercept of the linear correlation between the experimental shifts and the calculated shieldings. Calculations of all four molecules were done on completely optimized structures. Calculations on molecule **2** were also done on the available X-ray structure with only the hydrogen atom positions optimized. Correlations for compound **1** gave $R^2 = 0.9985$ and a standard error of 2.4 ppm, compound **2** gave $R^2 = 0.9969$ and a standard error of 3.55 ppm, compound **8** gave $R^2 = 0.9958$ and a standard error of 4.07 ppm, and compound **10** gave $R^2 = 0.9931$ and a standard error of 5.16 ppm.

Acknowledgment. This work was supported by the National Institutes of Health (Grants CA 36622 and RO1 AI26730). We thank Dr. Bill Baker (Florida Tech, FL) for the collection and donation of *Telesto riisei*, Dr. Bert Vogelstein (Johns Hopkins University, MD) for donation of the HCT 116 competent and null cell lines, Dr. Martin Rechsteiner (University of Utah) for supplying Ub−PEST, and Dr. Mark Meuth (University of Sheffield, U.K.) for the donation of the RKO and RKO-E6 cell lines. An allocation of computer time from the Center for High Performance Computing at the University of Utah is gratefully acknowledged. Low-resolution mass spectrometry was performed by Dr. Elliot Rachlin and was supported by the National Science Foundation (Grant CHE-9002690) and the University of Utah Funds Committee. (+)-HRESIMS measurements where provided by Dr. Lynn Teesch, Director, High Resolution Mass Spectrometry Facility, University of Iowa.

References

(1) Ishikawa, T.; Akimaru, K.; Nakanishi, M.; Tomokiyo, K.; Furuta, K.; et al. Anti-cancer-prostaglandin-induced cell-cycle arrest and its modulation by an inhibitor of the ATP-dependent glutathione S-conjugate export pump (GS-X) pump. *Biochem. J.* **1998**, *336*, 569−576.

(2) Straus, D. S.; Glass, C. K. Cyclopentenone prostaglandins: new insights on biological activities and cellular targets. *Med. Res. Rev.* **2001**, *21*, 185−210.

(3) Kato, T.; Fukushima, M.; Kurozumi, S.; Noyori, R. Antitumor activity of delta 7-prostaglandin A1 and delta 12-prostaglandin J2 in vitro and in vivo. *Cancer Res.* **1986**, *46*, 3538−3542.

(4) Narumiya, S. Structures, properties and distributions of prostanoid receptors. In *Advances in Prostaglandin Thromboxane and Leukotriene Research; Prostaglandins and Related Compounds*; Samuelsson, B., et al., Eds.; Raven Press: New York, 1995; Vol. 23, pp 17−22.

(5) Narumiya, S.; Sugimoto, Y.; Ushikubi, F. Prostanoid receptors: structures, properties, and functions. *Physiol. Rev.* **1999**, *79*, 1193−1226.

(6) Mullally, J. E.; Moos, P. J.; Edes, K.; Fitzpatrick, F. A. Cyclopentenone prostaglandins of the J series inhibit the ubiquitin isopeptidase activity of the proteasome pathway. *J. Biol. Chem.* **2001**, *276*, 30366−30373.
(7) Voges, D.; Zwickl, P.; Baumeister, W. The 26S proteasome: a molecular machine designed for controlled proteolysis. *Annu. Rev. Biochem.* **1999**, *68*, 1015−1068.
(8) Hershko, A.; Ciechanover, A. The ubiquitin system for protein degradation. *Annu. Rev. Biochem.* **1992**, *61*, 761−807.
(9) Wilkinson, K. D.; Tashayev, V. L.; O'Connor, L. B.; Larsen, C. N.; Kasperek, E.; et al. Metabolism of the polyubiquitin degradation signal: structure, mechanism, and role of isopeptidase T. *Biochemistry* **1995**, *34*, 14535−14546.
(10) D'Andrea, A.; Pellman, D. Deubiquitinating enzymes: a new class of biological regulators. *Crit. Rev. Biochem. Mol. Biol.* **1998**, *33*, 337−352.
(11) Mullally, J. E.; Fitzpatrick, F. A. Pharmacophore model for novel inhibitors of ubiquitin isopeptidases that induce p53-independent cell death. *Mol. Pharmacol.* **2002**, *62*, 351−358.
(12) Noyori, R.; Suzuki, M. Organic synthesis of prostaglandins: advancing biology. *Science* **1993**, *259*, 44−45.
(13) Suzuki, M.; Mori, M.; Niwa, T.; Hirata, R.; Furuta, K.; et al. Chemical implications for antitumor and antiviral prostaglandins: reaction of Δ^7-prostaglandin A_1 and prostaglandin A_1 methyl esters with thiols. *J. Am. Chem. Soc.* **1997**, *119*, 2376−2385.
(14) Kim, I.-K.; Lee, J.-H.; Sohn, H.-W.; Kim, H.-S.; Kim, S.-H. Prostaglandin A_2 and Δ^{12}-prostaglandin J_2 induce apoptosis in L1210 cells. *FEBS Lett.* **1993**, *321*, 209−214.
(15) Sasaki, H.; Fukushima, M. Prostaglandins in the treatment of cancer. *Anti-Cancer Drugs* **1994**, *5*, 131−138.
(16) Henschler, D.; Eder, E. Structure−activity relationships of α,β-unsaturated carbonylic compounds. *IARC Sci. Publ.* **1986**, *70*, 197−205.
(17) Rosen, J. D.; Segall, Y.; Casida, J. E. Mutagenic potency of haloacroleins and related compounds. *Mutat. Res.* **1980**, *78*, 113−119.
(18) Baker, B. J.; Okuda, R. K.; Yu, P. T. K.; Scheuer, P. J. Punaglandins: halogenated antitumor eicosanoids from the octocoral *Telesto riisei*. *J. Am. Chem. Soc.* **1985**, *107*, 2976.
(19) Baker, B. J.; Scheuer, P. J. The punaglandins: 10-chloroprostanoids from the octocoral *Telesto riisei*. *J. Nat. Prod.* **1994**, *57*, 1346−1353.
(20) Mynderse, J. S.; Bonjouklian, R. Anti-inflammatory method. *Chem. Abstr.* **1986**, 214107a.
(21) Fukushima, M.; Kato, T. Antitumor marine icosanoids: clavulones and punaglandins. Adv. Prostaglandin Thromboxane *Leukot. Res.* **1985**, *15*, 415−418.
(22) Dominguez, J. N.; Taddei, A.; Cordero, M.; Blanca, I. Synthesis of C(11)-halogenated prostaglandins. *J. Pharm. Sci.* **1992**, *83*, 472−475.
(23) Rogers, S.; Wells, R.; Rechsteiner, M. Amino acid sequences common to rapidly degraded proteins: the PEST hypothesis. *Science* **1986**, *234*, 364−368.
(24) Yoo, Y.; Rote, K.; Rechsteiner, M. Synthesis of peptides as cloned ubiquitin extensions. *J. Biol. Chem.* **1989**, *264*, 17078−17083.
(25) Mullally, J. E. Discovery of novel effectors of the proteasome pathway: cyclopentenones as inhibitors of ubiquitin isopeptidase activity. Ph.D. Thesis in *Medicinal Chemistry*; University of Utah: Salt Lake City, UT, 2003.
(26) Lopes, U. G.; Erhardt, P.; Yao, R.; Cooper, G. M. p53-dependent induction of apoptosis by proteasome inhibitors. *J. Biol. Chem.* **1997**, *272*, 12893−12896.
(27) Haupt, Y.; Maya, R.; Kazaz, A.; Oren, M. Mdm2 promotes the rapid degradation of p53. *Nature* **1997**, *387*, 296−299.
(28) Kubbutat, M. H. G.; Jones, S. N.; Vousden, K. H. Regulation of p53 stability by Mdm2. *Nature* **1997**, *387*, 299−303.
(29) Scheffner, M.; Werness, B. A.; Huibregtse, J. M.; Levine, A. J.; Howley, P. M. The E6 oncoprotein encoded by human papillomavirus types 16 and 18 promotes the degradation of p53. *Cell* **1990**, *63*, 1129−1136.
(30) Scheffner, M.; Huibregtse, J. M.; Vierstra, R. D.; Howley, P. M. The HPV-16 E6 and E6-AP complex functions as a ubiquitin-protein ligase in the ubiquitination of p53. *Cell* **1993**, *75*, 495−505.
(31) Ashcroft, M.; Vousden, K. H. Regulation of p53 stability. *Oncogene* **1999**, *18*, 7637−7643.
(32) Moos, P. J.; Edes, K.; Fitzpatrick, F. A. Inactivation of wild-type p53 tumor suppressor by electrophilic prostaglandins. *Proc. Natl. Acad. Sci. U.S.A.* **2000**, *97*, 9215−9220.
(33) Orlowski, R. Z. The role of the ubiquitin−proteasome pathway in apoptosis. *Cell Death Differ.* **1999**, *6*, 303−313.
(34) Alnemri, E. S.; Livingston, D. J.; Nicholson, D. W.; Salvesen, G.; Thomberry, N. A.; Wong, W. W.; Yuan, J. Human ICE/CED-3 protease nomenclature. *Cell* **1996**, *87*, 171.

JM030448L